# *Ab initio* ground state and $L_{2,3}$ x-ray magnetic circular dichroism of Mn-based Heusler alloys

I. Galanakis, S. Ostanin, M. Alouani, and H. Dreyssé
*IPCMS-GEMME, 23, rue du Loess, F-67037 Strasbourg Cedex, France*

J. M. Wills
*Center for Materials Science, Theoretical Division, Los Alamos National Laboratory, Los Alamos, New Mexico 87544*
(Received 29 June 1999)

Relativistic full-potential calculations within the generalized gradient approximation (GGA) for a series of Mn-based Heusler alloys are presented. Calculated equilibrium lattice parameters deviate less than 1.2% from the experimental values. The main features of a half metallic system are present in the density of states for the PtMnSb and NiMnSb. We predict that PdMnSb shows half metallic character under hydrostatic pressure. The substitution of Sb in PtMnSb by Sn or Te destroys the minority spin band gap. Spin and orbital magnetic moments for all the systems are in good agreement with previous calculations and experimental data. $L_{2,3}$ x-ray absorption and x-ray magnetic circular dichroism (XMCD) spectra are calculated for all the five compounds. Pt spectra present big deviations from system to system in the PtMn$Y$ ($Y$=Sn,Sb,Te) compounds while Mn spectra show only small deviations. For all these spectra GGA underestimates the $L_3/L_2$ integrated branching ratio and produces a much smaller $L_2$ peak intensity for the Ni site in NiMnSb. The XMCD sum rules are used to compute the spin and orbital magnetic moments and the results are compared to the direct calculations.

## I. INTRODUCTION

Magnetic ternary alloys of the $L2_1$ and $C1_b$ crystalline structure have attracted a lot of interest since they were studied by Heusler.[1] de Groot *et al.*[2] showed that these that crystallize in the $C1_b$ (MgAgAs type)[3] structure constitute an interesting class of materials. They predicted that NiMnSb and PtMnSb are half metallic ferromagnets, i.e., the majority spin (spin-up) band is metallic while the minority (spin-down) band is semiconducting, leading to 100% spin polarization at the Fermi level. They exhibit high value of saturated magnetic moment per Mn atom ($\sim 4\mu_B$) and a high Curie temperature.[4] Most experiments have been performed for PtMnSb which presents one of the highest polar-Kerr rotation angles among the magneto-optic metallic materials at room temperature.[5] Thin films of these materials can act as spin filters and enhance the performance of devices based on the giant magneto-resistance effect.[6] Only recently it has been made possible to grow such films because of the difficulty in obtaining a uniform, well ordered $C1_b$-type crystal structure and because of the sensitivity of their electronic structure to the lattice parameters.[6,7]

Calculations by Hanssen and Mijnarends[8] by means of a non-self-consistent Korringa-Kohn-Rostoker method and by Kulatov and Mazin[9] by means of a scalar-relativistic linear muffin-tin orbital (LMTO) (Ref. 10) method in its atomic sphere approximation (ASA) produced a half metallic behavior for NiMnSb. More recent spin-polarized band calculations[11,12] within the local spin-density approximation (LSDA) (Ref. 13) verified the half metallic nature of PtMnSb and NiMnSb. The band gaps have been found to depend strongly on the variation of the lattice parameters, and the spin-orbit interaction, while substantial for PtMnSb, it is found to be negligible for NiMnSb.[11] Kirillova and co-workers[14] analyzed the interband absorption based on experimental data and showed the presence of a small energy gap for four isostructural $X$MnSb ($X$=Cu,Pt,Pd,Ni) compounds. Ellipsometric evidence of the spin-down gap for PtMnSb was reported also recently.[15] However, impurity-type electronic-structure calculations for PtMnSb indicate that the lattice disorder has a ''dramatic impact on the spin polarization and the gap in the vicinity of the Fermi level''[16] thus explaining the reason photoemission experiments could find only a degree of the full polarization. Otto *et al.*[17] have measured the Hall effect of several $X$MnSb compounds and showed that in the case of Heusler alloys the asymmetric scattering of the charge carriers is mainly due to spin-disorder scattering and not to orbital scattering. Finally, Gao *et al.*[18] have calculated the dielectric tensor for the NiMnSb system and showed that the high-energy Kerr rotation peak arises only from transitions involving spin-orbit coupling.

Antonov *et al.* have studied the magneto-optic properties of 15 ternary ferromagnetic $C1_b$- and $L2_1$-type compounds.[19] The large Kerr effect on PtMnSb was attributed to the simultaneous existence of the gap in the minority-spin band, the big magnetic moment $\sim 4\mu_B$ at the Mn site, and the large spin-orbit coupling at the Pt site. van Ek *et al.* showed in the case of Pt(Ni)MnSb that the polar-Kerr effect for red light is independent from the half metallic properties of these compounds.[20]

The dichroism-type spectroscopy became a powerful tool in the study of the electronic structure of magnetic materials.[21,22] The x-ray-absorption spectroscopy (XAS) using polarized radiation probes element specific magnetic properties of alloys and compounds via the x-ray magnetic circular dichroism (XMCD) by applying the sum rules to experimental spectra.[23–25] The application of these sum rules to itinerant systems, in particular to low symmetry systems, is debated since the sum rules are derived from atomic theory.[24,26,27] In particular, the XAS and XMCD spectra have been measured recently in the Mn $2p$ core absorption region for MnSb-based Heusler alloys and for Ni in the NiMnSb.[28]

 

Several *ab initio* calculations have been performed trying to understand theoretically the XMCD. Most of them concern the $3d$ transition metals,[27,29,30] involving electronic excitations of $2p_{1/2}$ ($L_2$ edge) and $2p_{3/2}$ ($L_3$ edge) core electrons towards *d*-valence states. The XMCD signal depends on the exchange splitting and the spin-orbit coupling of both initial core and final valence states. Brouder and co-workers,[31] Guo,[32] and Ankudinov and Rehr[33] used multiple-scattering theory to study XMCD but their method, although successful, has been only applied to systems with few atoms per unit cell, as their formalism is computationally involved. Finally, atomic calculations, using crystal-field symmetry, are widely applied to fit the experimental $M_{4,5}$ edges of rare earths and actinide compounds and the $L_{2,3}$ edges of early transition metals. Because of the large number of parameters to fit, it is difficult to apply this formalism to delocalized $3d$ states.[34]

In this paper we focus on the study of five Heusler compounds: PtMnSn, PtMnSb, PtMnTe, PdMnSb, and NiMnSb. In Sec. II we present briefly the theoretical method used to calculate the orbital magnetic moment, the absorption coefficients for the circularly polarized x-ray radiation and the details of the calculations. The equilibrium lattice properties are presented in the Sec. III. In Sec. IV we discuss the electronic structure of these compounds and the magnetic properties. In Sec. V we calculate the XAS and XMCD spectra and we compare them to experiments. In Sec. VI we use the sum rules to determine the spin and orbital moments and compare them to direct calculations. A particular interest is devoted to the behavior of the Pt and Mn atoms in the different Heusler compounds.

## II. THEORETICAL MODEL

To calculate the band structure we used the relativistic full-potential linear muffin-tin orbital method (FP-LMTO) method.[35] The space within this method is divided in two regions: the nonoverlapping spheres [muffin-tin (MT) spheres] centered in each atom and the interstitial region. The muffin-tin potential is developed over the lattice harmonics of the system and the rest of the potential is treated using fast Fourier transform (FFT). The core electrons are spin polarized and their electronic states are obtained by solving iteratively the Dirac equation. For the valence electrons the spin-orbit coupling is added to the semirelativistic Hamiltonian; and the total Hamiltonian is solved self-consistently.

If $D^{\tau}_{l,m_l,\sigma}(E)$ is the projected density of states on each muffin-tin sphere $\tau$ and on the $l$, $m_l$, $\sigma$ basis (where $l$, $m_l$ are the angular momentum quantum numbers and $\sigma$ the spin), to calculate the average orbital magnetic moment $\langle m^l_{\tau,orb}\rangle$ of the atom $\tau$, we use the expression

$$\langle m^l_{\tau,orb}\rangle = \sum_{\sigma} \sum_{m_l} m_l \int_{-\infty}^{E_F} D^{\tau}_{l,m_l,\sigma}(E)\,dE. \tag{1}$$

The integral is taken up to the Fermi level $E_F$.

In order to calculate the matrix elements and consequently the absorption coefficients for left $\mu_+$ and right $\mu_-$ circular polarized x-ray radiation, we use the dipole approximation to the electron-photon interaction $\hat{\mathbf{e}}_{\pm}\mathbf{p} = (1/\sqrt{2})(\nabla_x \pm i\nabla_y)$, where $e_{\pm}$ is the polarization vector. We also consider the spin-quantization axis along the direction of the x-ray beam like in XMCD experiments. The absorption at the $j_{\pm}$ ($l \pm \frac{1}{2}$) core edge is given by the relation

$$\mu_{\pm}(\omega) = \frac{2\pi}{\hbar} \sum_{m_{j_{\pm}}} \sum_{n,\mathbf{k}} \langle j_{\pm} m_{j_{\pm}} | \hat{\mathbf{e}}_{\pm}\mathbf{p} | n\mathbf{k}\rangle \langle n\mathbf{k} | \mathbf{p}\hat{\mathbf{e}}_{\pm} | j_{\pm} m_{j_{\pm}}\rangle \times \delta(\omega - E_{n\mathbf{k}} + E_{j_{\pm}}), \tag{2}$$

where the first sum runs over the initial core states and the second one over the unoccupied final states. The XMCD spectrum is defined as the difference between the left and right absorption coefficient for each x-ray energy.

All calculations are performed within the generalized-gradient approximation[36] (GGA) to the exchange-correlation potential. To develop the potential inside the MT spheres we calculated a basis set of lattice harmonics including functions up to $l=8$, while for the FFT we used in real space a grid of $48\times48\times48$. The Brillouin-zone integrations during the self-consistency are performed by means of a Gaussian smearing of 0.1 eV width and 256 **k** points in the Brillouin zone (88 in the irreducible part). We treated the Mn $3p$, Sb $4d$, Ni $3p$, Pd $4p$, and Pt $5p$ states as semicore. For the valence electrons we used a basis set containing $3\times s$, $3\times p$, and $2\times d$ wave functions. The spin axis was chosen to be along the [111] direction, which is the easy magnetization axis of these Heusler alloys, contrary to all previous calculations that used the [001] as quantization axis. Similar investigation for Fe, Fe nitrides,[30] CoPt,[37] and FePd (Ref. 38) compounds were in good agreement with experiment.

TABLE I. Calculated equilibrium lattice constants $a_0$ (in Å) compared to experimental lattice constants by Otto *et al.* (Ref. 39) (second line) and by van Engen *et al.* (Ref. 5) (third line). The difference between calculated and experimental lattice constants does not exceed 1.2%.

| | NiMnSb | PdMnSb | PtMnSn | PtMnSb | PtMnTe |
|---|---|---|---|---|---|
| $a_0$ | 5.923 | 6.231 | 6.187 | 6.227 | 6.346 |
| $a_{exp}$ (Otto) | 5.927 | | 6.261 | 6.195 | |
| $a_{exp}$ (van Engen) | 5.920 | 6.285 | 6.264 | 6.210 | |

## III. EQUILIBRIUM LATTICE PROPERTIES

The absence of experimental lattice parameters for the PtMnTe has motivated us to determine these parameters by minimization of the the total energy. All the calculations have been performed within the GGA because this approximation to the exchange-correlation potential is known to produce better lattice properties than LSDA. In Table I we compare our results with experimental results of Otto *et al.*[39] for PtMnSn, PtMnSb, and NiMnSb alloys.[40] For the NiMnSb the agreement is practically perfect (5.923 Å, theory, compared to 5.927 Å, experiment). For PtMnSb our theory overestimates the lattice parameter by 0.5%, while for PtMnSn it underestimates it by 1.1%. Similar experiments by van Engen *et al.*[5] produced the same lattice parameters within less than 1%. Since the agreement of the lattice parameters with

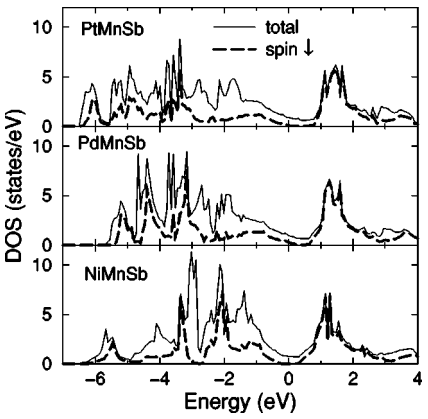


FIG. 1. Total and spin-down projected density of states for the three Sb-based Heusler compounds. All the DOS show similar characteristics but the PdMnSb does not present a half metallic behavior and has a 1-eV smaller bandwidth.

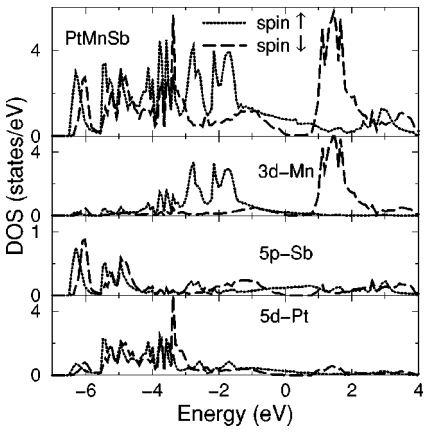


FIG. 2. Spin and atom projected density of states for the PtMnSb calculated using the experimental lattice constant. The large exchange splitting of the Mn $3d$ states leads to a large localized spin magnetic moment ($\sim 4\mu_B$) at the Mn site and to the polarization of the Mn $3d$ bands away from the Fermi level. The Pt $5d$ and Sb $5p$ states lay lower in energy.

experiment is less than 1.2%, we expect that our lattice parameter for PtMnTe (6.346 Å) is a good prediction.

For the Pt-based compounds, valence electrons are gradually added to the system when Sn is substituted by Sb or Te resulting in an increase of the lattice parameter. It is surprising that this behavior is not seen in experiment. This could be due primarily to the stronger atomic disorder in the PtMnSn system as compared to PtMnSb sample.[17] For all the rest of the calculations we used the experimental lattice parameters measured by Otto for PtMnSb, NiMnSb, and PtMnSn, and the experimental value of van Engen for PdMnSb. For PtMnTe we used our calculated equilibrium lattice constant.

## IV. DENSITY OF STATES AND MAGNETIC MOMENTS

The electronic structures of the NiMnSb and PtMnSb compounds have been extensively reported in the literature,[2,11,19,42] so in this section we briefly discuss the most important features on their density of states (DOS) curves and will concentrate essentially on the electronic structure trends of the Pt-based alloys and of PdMnSb. In all DOS plots the Fermi level is taken to be the zero of the energy scale.

Figure 1 shows the total and the spin-down density of states for the three Sb-based Heusler alloys. The most studied alloy is the NiMnSb as it was the first $C1_b$-type alloy investigated by de Groot *et al.*[2] As it is already known and verified by our full-potential calculations the density of states is dominated by a large exchange splitting ($>3$ eV) between the spin-up and the spin-down bands of the Mn $3d$ states. This is clearly seen in the atomic projected density of states[41] for the PtMnSb system shown in Fig. 2. Similar DOS is obtained for the Mn $3d$ band in the other two alloys, NiMnSb and PdMnSb. This large exchange splitting leads to large localized spin magnetic moments ($\sim 4\mu_B$) at the Mn site and to the polarization of the Mn $3d$ bands away from the Fermi level. We can essentially identify three peaks. The peak over the Fermi level comes from the spin-down band and the double peak structure below the Fermi level is due to the exchange interaction.

For PtMnSb the minority spin DOS shows a gap just at the vicinity of the Fermi level that is in agreement with previous relativistic calculations.[11,19,42] Notice, that the Fermi level is placed just at the edge of the half metallic gap for PtMnSb alloy. Based on a scalar-relativistic calculation for NiMnSb, Kulatov and Mazin[9] argued that the exact position of the Fermi level with respect to the half metallic gap cannot be reliably determined within the density-functional theory[43] and it depends strongly on the approximation to the exchange-correlation potential that is used.[42] But this strong claim is not confirmed by our calculations. In particular, the position of the Fermi level with respect to the gap for both PtMnSb and NiMnSb within our calculations (FP-LMTO, GGA), calculations of Antonov *et al.*[19] (LMTO-ASA, LSDA), and the calculations of Youn and Min[11] (LMTO-ASA, LSDA) is the same, at the middle of the gap for the NiMnSb and at the lower energy side of the gap for PtMnSb, although in all the three calculations different numerical codes and different exchange-correlation potentials are used. The common point between the three calculations is the treatment of the spin-orbit coupling. So it seems that the claim of Kulatov and Mazin is not due to exchange-correlation approximation but to the neglect of the spin-orbit coupling in their calculations. Pt $5d$ states are practically filled for both spin directions, and lay lower in energy than the Mn $3d$ states, because Pt has a bigger atomic number. This results on a smaller hybridization between Mn $3d$ and Pt $5d$, which leads to a small induced magnetic moment on the Pt site ($0.10\mu_B$). The Sb valence states are mainly $5s$ and $5p$ states and are weakly antiferromagnetically coupled to the Mn $3d$ states so that the induced magnetic moment on the Sb site is only $-0.07\mu_B$.

NiMnSb shows similar behavior as PtMnSb but the spin-orbit coupling plays a lesser important role due to the much smaller atomic number of Ni as compared to Pt.[11] The Fermi level lies in the middle of the spin-down gap enabling half metallic properties of this alloy. The spin-up DOS in a region of about 1 eV around the Fermi level is similar for all the three Sb-based compounds. The Ni $3d$ bands are far from the Fermi level and are almost filled for both spin directions resulting in a small spin magnetic moment of $0.26\mu_B$. Our

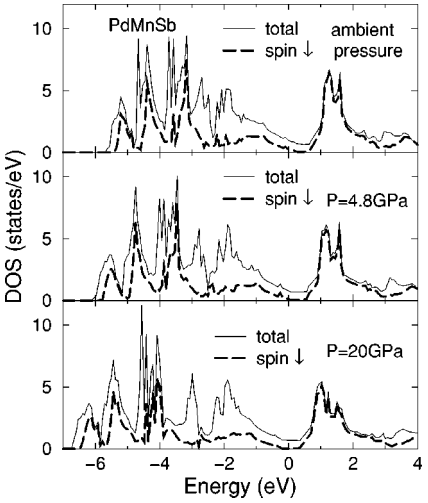


FIG. 3. Total and minority spin projected density of states (DOS) for PdMnSb at ambient pressure and for two sets of reduced lattices constants. Under hydrostatic pressure there is a slight rearrangement of the electrons in the DOS and PdMnSb presents half metallic properties. Notice that the bandwidth under pressure is now closer to that of PtMnSb and NiMnSb at ambient pressure.

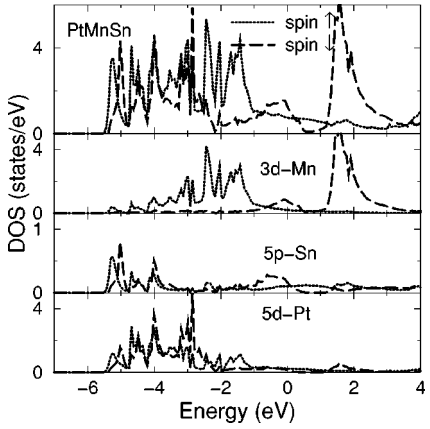


FIG. 4. The same plot as Fig. 2 but for PtMnSn. The density of states (DOS) for PtMnSn has similar features as for PtMnSb but the one electron reduced number of valence electrons moves the position of the Fermi level towards lower energies, so that instead of a pure energy gap in the spin-down DOS there is a region of very small DOS of 0.6-eV bandwidth starting from the Fermi level.

value is in good agreement with that of Youn and Min.[11] The Sb site is weakly antiferromagnetically coupled to the other two atoms as in the case of PtMnSb.

A very different situation is obtained in the case of PdMnSb; it presents no half metallic character in agreement with previous calculations by Antonov *et al.*[19] and as was initially predicted by de Groot *et al.*[2] Although PdMnSb DOS (see Fig. 1) has essentially the same form as that of the PtMnSb and NiMnSb DOS the occupied part starts at about 1 eV above these two Heusler alloys. The low-energy part of the DOS is dominated by the Pd $4d$ and the Sb $5p$ states, so this difference should be attributed to stronger hybridization between these orbitals. For this system Mn shows the strongest polarization of the Sb-based compounds resulting in a spin magnetic moment of $4.03\mu_B$. Pd $4d$ states show the same behavior as Ni $3d$ and Pt $5d$ states and spin induced magnetic moment at the Pd site is $0.09\mu_B$, while Sb has a similar but negative moment ($-0.09\mu_B$). There is a narrow energy-band gap of spin-down states at around 0.5 eV above the Fermi level. It seems that the half metallic behavior of PdMnSb alloy, which is not present at ambient pressure, could appear under strain or hydrostatic pressure conditions where the Fermi level could be moved inside the gap. To verify this assumption we calculated the DOS for the PdMnSb under an hydrostatic pressure of 4.8 and 20 GPa and the resulting DOS is presented in Fig. 3. 4.8 GPa of hydrostatic pressure corresponds to 5% reduction of the unit-cell volume compared to the ambient pressure unit cell and 20 GPa corresponds to 15%. Thus PdMnSb under pressure shows a quite large band gap in the spin-down states like the other half metallic Heusler alloys. We can see that as the pressure increases this gap becomes larger. The Fermi level changes position and for 4.8 GPa hydrostatic pressure it is situated at the lowest energy side of the gap, while for 20 GPa it is situated at the middle of the gap. These two situations correspond exactly to PtMnSb and NiMnSb behavior, respectively. Apart from the change in the position of the Fermi level the only change in the DOS concerns the lowest occupied valence states that are dominated by the Pd $4d$ and the Sb $5p$ states. The hydrostatic pressure effect leads to a decrease in the magnetic moment of Mn; reducing it from $4.03\mu_B$ for ambient pressure to $3.91\mu_B$ for 4.8 GPa pressure and further to $3.78\mu_B$ for 20 GPa. The compression increases the hybridization between the Mn $3d$ states and the Pd $4d$ leading to an increase of its induced magnetic moment. Pd spin magnetic moment changes from $0.09\mu_B$ at ambient pressure to $0.10\mu_B$ for 4.8 GPa and $0.16\mu_B$ for 20 GPa. The magnetic coupling between the Sb and the other two sites for 20 GPa pressure becomes ferromagnetic (Sb spin magnetic moment becomes $0.12\mu_B$).

In the next step we study the behavior of the Pt-based ternary alloys by substituting Sb by Sn that has one valence electron less or by Te that has one valence electron more. Substituting Sb in PtMnSb alloy by Sn has a rather expected consequences (see in Fig. 4). The DOS has similar features as for PtMnSb but the smaller number of valence electrons lowers the position of the Fermi level. The spin-down band gap is pushed towards higher energies by about 0.6 eV in agreement with the results of Halilov and Kulatov[42] and contradicting the results of Antonov *et al.*[19] that found a pure gap in this region. The spin-down density of states at the Fermi level is larger than for the spin-up band as predicted by de Groot *et al.*[2] The most important change concerns the induced magnetic moment at Pt site which vanishes for the PtMnSn compound and the hybridization between the Mn $3d$ states and the Sn $5s$ and $5p$ electrons becomes more important leading to a slight decrease of the magnetic moment at the Mn site ($3.88\mu_B$ in the case of PtMnSn compared to $3.93\mu_B$ for PtMnSb). We notice also a slight increase of the absolute value of the spin magnetic moment at the Sn site compared to that of Sb ($-0.11\mu_B$ compared to $-0.07\mu_B$). Our calculated Mn moment is slightly higher than the one calculated by de Groot *et al.*[2] ($3.60\mu_B$).

The PtMnTe compound has not yet been studied experimentally principally because of the difficulty in preparing Te-based compounds and hence no calculations has been done for this compound. For reasons of completeness we

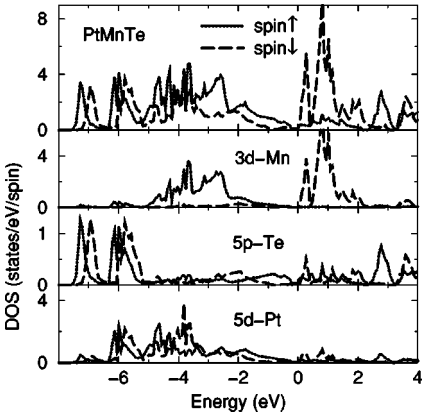


FIG. 5. The same plot as Fig. 2 but for PtMnTe. Substituting Sb in PtMnSb alloy by Te has a rather complex consequence. There is a double peak structure for the Mn $3d$ up states which is not seen in the other four compounds. The total density of states is very low exactly before the Fermi level leading to a semimetallic behavior.

discuss also this alloy. As can be seen in Fig. 5, substituting Sb in PtMnSb alloy by Te has a rather complex consequence. There is a double peak structure for the Mn $3d$ up states contrary to all the other four compounds. The very low total DOS in a region of 0.2 eV just before the Fermi level leads to a semimetallic behavior. The origin of this low DOS is traced back to the bigger exchange splitting of the Mn $3d$ states in PtMnTe, which via hybridization affects also the Pd $4d$ and Sb $5p$ states. Spin magnetic moment at the Mn site gets its higher value of $4.29\mu_B$. The induced spin magnetic moment at the Pt site is $0.26\mu_B$ which is more than the double of the PtMnSb value. Te presents a ferromagnetic coupling with the Mn contrary to all the other compounds of the *X*Mn*Y* type where the Y atom is antiferromagnetically coupled to the Mn.

In Table II we have gathered the calculated spin magnetic moments for all the compounds together with previous results of Youn and Min[11] within LMTO-ASA.[10] In the third column we present the values obtained by Kimura *et al.*[28] by applying the sum rules to their spectra. For PtMnSn system the Mn spin magnetic moment has been measured by Kirillova *et al.*,[14] and it is the only case where the experimental value is much smaller than the calculated value. Such deviations are expected because our calculations are performed for zero temperature while experiments are performed for finite temperatures, where spin fluctuations are important. This causes a reduction of the projection of the spin magnetic moment on the spin quantization axis and so an overestimation of the spin magnetic moment with respect to experiment. The discrepancy can come also partially from the bigger atomic disorder that PtMnSn samples present compared to the other compounds.[17,39] Magnetic moments in the interstitial region (of the order of $\pm 0.05\mu_B$) are small compared to the moment at the Mn site but important compared to the other atoms. The open structure of *X*Mn*Y* leads to a larger interstitial region since in our method the muffin-tin spheres are not allowed to overlap. There is no easy way to attribute the interstitial electrons to any particular atom of the alloy.

In Table II we also present the orbital magnetic moments of the *d* states for Ni, Mn, Pd, and Pt and the orbital magnetic moments of the *p* states for Sb, Sn, and Te. For the Mn atom and for all the compounds with the exception of PtMnTe we found a value of $0.04\mu_B$ in good agreement with previous calculations by Wang *et al.*,[12] that used a tight-binding (TB) version of the LMTO-ASA method. The $\langle m_{orb}\rangle/\langle m_{spin}\rangle$ for these four compounds is 0.01 in agreement with Kimura *et al.*[28] that predicted that this value should be less than 0.05. The calculated value is an underestimation of the real value because it is already known that both LSDA and GGA significantly underestimate the orbital magnetic moment,[44] but manage to represent the correct trends.[37] Pt orbital moment presents a big anisotropy between different compounds reflecting the differences in the crystal field as we substitute Sn by Sb or Te. The same argument is also suitable for the *p* projected orbital magnetic moment of Sb in the different compounds. The only discrepancy between our full-potential calculations and these of Wang *et al.* concerns Pt atom in PtMnSb, for which the sign between the two calculations is different. This discrepancy should be attributed to the use of ASA in their calculations. In ASA calculations only the spherical part of the potential is used which is a poor approximation for highly anisotropic crystalline structures like the $C1_b$. ASA worked well for the band structure and the spin magnetic moments, but it cannot correctly treat properties that are very sensitive to the crystalline-field-like magnetocrystalline anisotropy or orbital

TABLE II. In the first column we present our calculated results for the atom-averaged spin magnetic moment $\langle m_{spin}\rangle$ in $\mu_B$ and in the second column Youn and Min (Ref. 11) calculated values by means of the LMTO-ASA method (Ref. 10). In the third column we show the spin magnetic moments extracted from the experimental XMCD spectra using the sum rules (Ref. 28), except for the PtMnSn where we show the value measured by Kirillova *et al.* (Ref. 14). The latest value is the only one that is significantly overestimated by our calculations. Here we expect spin fluctuations and intrinsic atomic disorder of the PtMnSn samples to play an important role. The fourth column represents the *d*-orbital magnetic moments except for Sb, Sn, and Te where we used the *p*-orbital moment values, because the valence electrons of these atoms are principally of *p* character. Finally, the last column shows the orbital magnetic moments calculated by Wang *et al.* (Ref. 12) within the TB-LMTO-ASA.

| | | $\langle m_{spin}\rangle$ FP | $\langle m_{spin}\rangle$ ASA | $\langle m_{spin}\rangle$ expt | $\langle m^d_{orb}\rangle$ FP | $\langle m_{orb}\rangle$ TB-ASA |
|---|---|---|---|---|---|---|
| | Ni | 0.26 | 0.26 | | 0.01 | 0.02 |
| NiMnSb | Mn | 3.72 | 3.76 | 3.85 | 0.04 | 0.03 |
| | Sb | −0.06 | −0.07 | | −0.01($p$) | ∼0 |
| | Pd | 0.09 | | | −0.08 | |
| PdMnSb | Mn | 4.03 | | 3.95 | 0.04 | |
| | Sb | −0.09 | | | 0.02($p$) | |
| | Pt | 0.10 | 0.08 | | −0.05 | 0.03 |
| PtMnSb | Mn | 3.93 | 3.97 | 4.02 | 0.04 | 0.05 |
| | Sb | −0.07 | −0.09 | | 0.01($p$) | ∼0 |
| | Pt | 0.01 | | | −0.14 | |
| PtMnSn | Mn | 3.88 | | 3.57 | 0.04 | |
| | Sn | −0.11 | | | 0.01($p$) | |
| | Pt | 0.26 | | | 0.12 | |
| PtMnTe | Mn | 4.298 | | | 0.02 | |
| | Te | 0.08 | | | −0.02($p$) | |

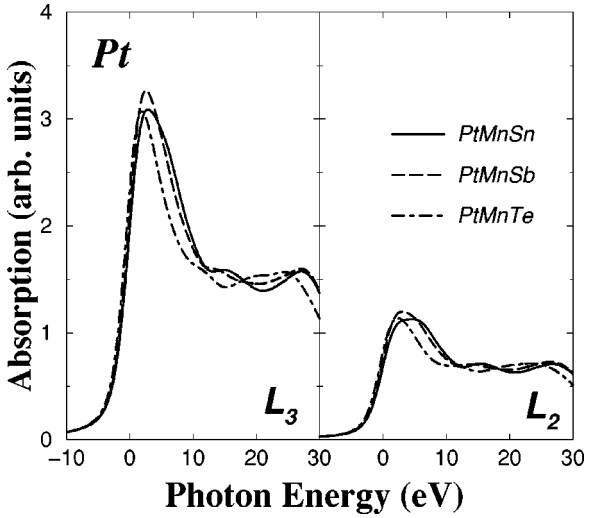


FIG. 6. X-ray absorption at the Pt site in the Pt-based compounds. There are slight changes but no general tendency can be observed.

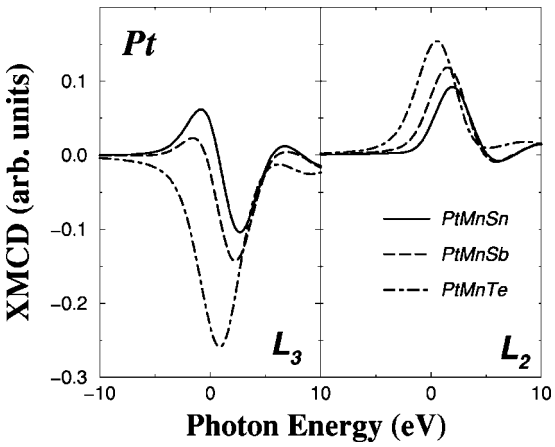


FIG. 7. XMCD spectra for the Pt atom in the three Pt-based alloys. The spectra of PtMnSn and PtMnSb have the same characteristics while the PtMnTe spectra has a different form, which is due to the underlying local magnetic properties of Pt in these alloys (see Table II).

magnetic moment where the nonspherical parts of the potential play an important role.

### V. X-RAY ABSORPTION AND DICHROISM

The last part of our work concerns the XAS and the XMCD of the Heusler alloys. To our knowledge only the Mn and Ni XMCD at the $L_{2,3}$ edges of NiMnSb and PtMnSb have been measured by Kimura *et al.*[28] It is of interest to mention that no information about the quality of the structural properties of these samples is known.[28] We concentrate first on the behavior of Pt in the three Pt-based compounds, then we discus the Mn spectra and in the last paragraphs the Ni and Pd behavior. For all the atoms except Pt we broadened the theoretical spectra by a Lorentzian of 0.9 eV width and a Gaussian of 0.4 eV to account for the core-hole life time broadening and the experimental resolution, respectively. As the lifetime of the hole in the Pt $2p$ core states is smaller than for the $3d$ ferromagnets the broadening used to account for the core hole would be larger; we then used a Gaussian of 1 eV width and a Lorentzian of 1 eV.[37] But the broadening does not change the integrated $L_3/L_2$ branching ratio. In the case of Pt, the $2p$ core states are very deep due to its bigger atomic number in comparison to Ni and Mn and hence screening of the core hole is weaker. The final state $\Psi_f$ wave function that the photoexcited electron sees in reality is not much different from the GGA calculated state $\Psi_i$. The discrepancy between theory, which approximates $\Psi_f$ by $\Psi_i$, and experiment is expected to be less important.[37]

In Figs. 6 and 7 we present the XAS and XMCD spectra, respectively, for the three Pt-based compounds. As we substitute Sn by Sb and then by Te, we successively add one electron more to the valence electrons, and we notice that this additional electron changes substantially the form of the XMCD spectra while the XAS are only slightly affected. PtMnSn and PtMnSb XMCD spectra have similar characteristics, in particular they exhibit a kink at the lower energy side of the $L_3$ edge and at the higher energy side of the $L_2$ edge. The intensities are much higher for the PtMnSb than for Pt in PtMnSn and so does the $L_3/L_2$ integrated branching ratio, 0.93 for PtMnSb and 0.40 for PtMnSn. The XMCD spectra of Pt in PtMnTe presents no kinks. The intensity of the $L_3$ edge is considerably higher than for the other two compounds, and that is also the case for the $L_3/L_2$ integrated branching ratio ($L_3/L_2=1.73$). This important difference in the behavior of the Pt atom in the three compounds is directly connected to the size of the local magnetic moment. A larger magnetic moment of Pt in PtMnTe ($0.026\mu_B$) results in a higher XMCD intensity and a smaller magnetic moment for Pt in PtMnSn ($0.01\mu_B$) results in a lower intensity.

In Fig. 8 we plot the calculated and experimental XAS and XMCD spectra for the Mn $L_{2,3}$ edges in NiMnSb and PtMnSb. As far as the absorption spectra are concerned the theory represents well the experimental features and overestimates slightly the $L_2$ edge intensity. The deviation from experiment is more important for the Ni-based system than for the Pt-based one. The energy difference between the $L_2$ and $L_3$ edge represents the size of the spin-orbit splitting of

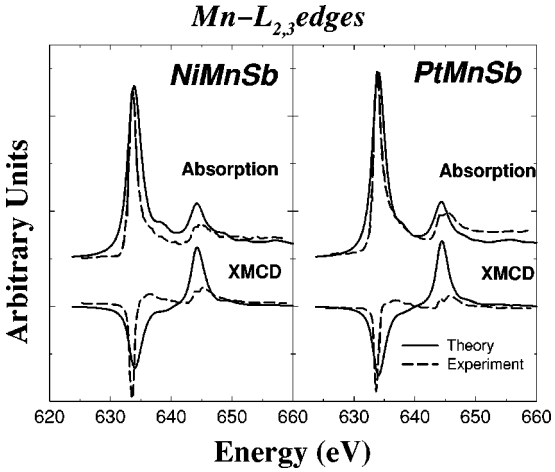


FIG. 8. Mn $L_{2,3}$ calculated and experimental 28 absorption and XMCD edges in the NiMnSb and PtMnSb compounds. Our calculation reproduces rather well the absorption but underestimates the $L_3/L_2$ integrated branching ratio.

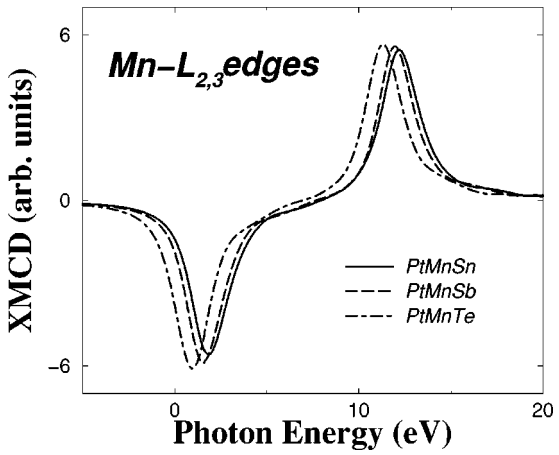


FIG. 9. Mn $L_{2,3}$ edges in the Pt-based compounds. Spectra change slightly with the compound but as the number of valence electrons increases, the $2p$ core states gets deeper.

the $2p$ core states, and experiment and theory give a value of about 10.5 eV. For both systems the theory underestimates the $L_3/L_2$ integrated branching ratio. The discrepancy is also more important for the Ni-based system than for the PtMnSb, and it is most probably due to the neglect of the core-hole effect.[45] Another source of discrepancy is the partial disorder of the sample used in the experiment. The disorder is not treated within our calculation and in the case of FePd it contributed significantly to the XMCD spectral shape.[46]

Figure 9 shows the calculated XMCD spectra for the Mn site through out the three Pt-based systems. The XAS spectra are almost identical and we have chosen not to plot them. We observe minor changes in the spectra. Intensities and $L_3/L_2$ integrated branching ratios increase slightly as we pass from the Sn-based alloy to the Te-based one ($L_3/L_2 = 1.02$ for PtMnSn and 1.08 for PtMnTe). The spin-orbit splitting of the $2p$ core states is identical for the three compounds, which is expected, but the relative position of the peaks changes. As an electron is added to the system, the $2p$ core states of Mn are affected and are pushed towards lower

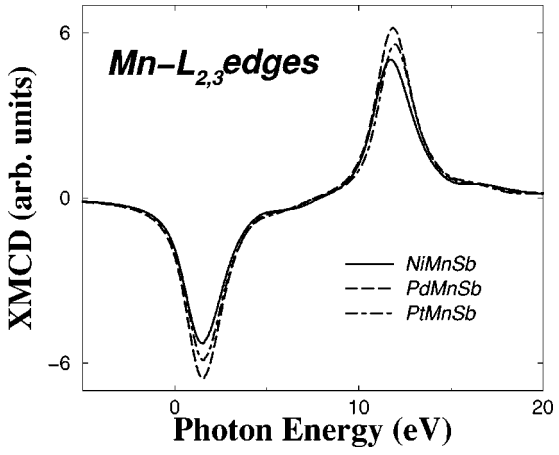


FIG. 10. Mn $L_{2,3}$ XMCD edges in the Sb-based alloys. The three Sb-based compounds, contrary to the three Pt-based compounds, have the same number of valence electrons, so the peaks are located in the same energies.

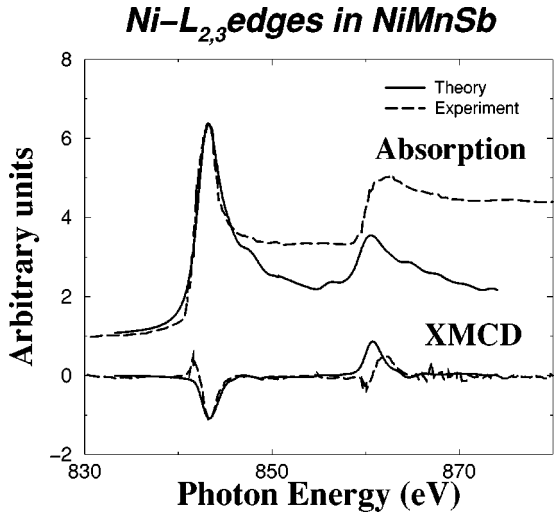


FIG. 11. Calculated and experimental Ni $L_{2,3}$ absorption and XMCD edges in NiMnSb. Our calculation strongly underestimates the $L_2$ absorption peak and fails to describe the kinks in the lower energy side of the XMCD edges.

energies. This change is about 1 eV when we move from PtMnSn to PtMnTe.

Figure 10 shows the calculated XMCD spectra for the Mn site but this time through out the Sb-based systems. There is no general tendency for the intensities and the $L_3/L_2$ integrated branching ratio and it remains constant, 1.03 for NiMnSb, 1.06 for PdMnSb, and 1.08 for PtMnSb. The three Sb-based compounds contrary to the three Pt-based compounds have the same number of valence electrons. This results on the same photon energy positions of the peaks in the XMCD spectra (Fig. 10).

The discrepancy between experiment and theory for the Ni site in NiMnSb is important even in the x-ray-absorption spectra (see Fig. 11). The theory underestimates the $L_2$ edge intensity by more than 50%. The XMCD spectrum does not reproduce the kink in the vicinity of each edge. The origin of these two kinks is probably the partial disorder of the sample used in experiments.[46] The calculated spin-orbit splitting of the Ni $2p$ core states is 17.6 eV, while it seems slightly larger in the experimental XAS.

In Fig. 12 we represent the absorption and XMCD for the

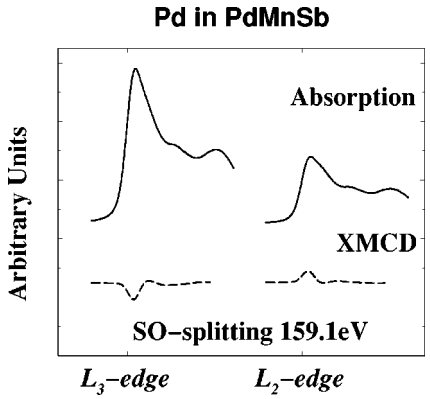


FIG. 12. Calculated x-ray total absorption and XMCD of the $L_2$ and $L_3$ edges for Pd in PdMnSb. The integrated $L_3/L_2$ XMCD branching ratio is 1.42.

TABLE III. Direct calculations of atom-averaged spin $\langle m_{spin}^{direct}\rangle$ and orbital $\langle m_{orb}^{direct}\rangle$ magnetic moments using Eq. (1) for NiMnSb and PtMnSb together with the ones derived by applying the sum rules to the theoretical XMCD spectra. From the sum rules we can derive the effective spin magnetic moment [see Eq. (4)]. The fifth column shows the number of holes $n_h$ in the *d* band used in Eqs. (3) and (4) and the last column the energy cutoff $E_{cutoff}$ of the integrals in these equations.

| | | $\langle m_{spin}^{direct}\rangle$ | $\langle m_{spineff}^{sumrul.}\rangle$ | $\langle m_{orb}^{direct}\rangle$ | $\langle m_{orb}^{sumrul.}\rangle$ | $n_h$ | $E_{cutoff}$ (eV) |
|---|---|---|---|---|---|---|---|
| NiMnSb | Ni | 0.26 | 0.31 | 0.01 | 0.01 | 1.51 | 4 |
| | Mn | 3.72 | 3.62 | 0.04 | −0.03 | 4.88 | 6 |
| PtMnSb | Pt | 0.10 | 0.11 | −0.05 | −0.07 | 2.33 | 6 |
| | Mn | 3.93 | 3.70 | 0.04 | 0.05 | 4.82 | 6 |

two Pd $L_{2,3}$ edges. The $L_3$ edge in the x-ray-absorption spectra is more than twice more intense than the $L_2$ peak. For the XMCD the $L_3/L_2$ integrated branching ratio is 1.42. The spin-orbit splitting is 159.1 eV and it is very close to the value for pure Pd of 160 eV. Since the core states are not considerably affected by the crystalline environment, it is then expected that the spin-orbit splitting remains practically unchanged in different Pd alloys.

To conclude this part regarding our calculated XAS and XMCD spectra we should stress that the agreement with experiment is only at the *qualitative* level, and that the one-electron theory is incapable of producing the correct XMCD branching ratio. We have invoked many reasons for this disagreement: (i) the one-electron theory neglects the effect of the core-hole photo-electron interaction. (ii) it neglects also the multi-electron processes such as the Coster-Kronig decay processes. (iii) the samples have intrinsic atomic disorder which is expected to play an important role. It is, however, interesting to notice that the calculated XAS Mn $L_{2,3}$ in both NiMnSb and PtMnSb are *similar* whereas the experimental ones are not, especially at the high energy side of the $L_2$ spectrum. We believe that further theoretical work is needed to better account for the details of the experimental XMCD spectra. Nevertheless our calculations constitute a good starting point for the understanding of the excited states of the Heusler alloys.

## VI. XMCD SUM RULES

XMCD sum rules have been derived by using an ion model by Thole *et al.*[23] and by Carra *et al.*[24] for atoms and by Ankudinov and Rehr[47] and Guo[32] in the case of solids. For the $L_{2,3}$ edges they take the following form:

$$\frac{\int_{L_2+L_3} d\omega[\mu_+(\omega)-\mu_-(\omega)]}{\int_{L_2+L_3} d\omega[\mu_+(\omega)+\mu_-(\omega)+\mu_0(\omega)]}=\frac{\langle L_z\rangle}{2n_h}, \qquad (3)$$

$$\frac{\int_{L_3} d\omega[\mu_+(\omega)-\mu_-(\omega)]-2\int_{L_2} d\omega[\mu_+(\omega)-\mu_-(\omega)]}{\int_{L_2+L_3} d\omega[\mu_+(\omega)+\mu_-(\omega)+\mu_0(\omega)]}=\frac{\langle S_z\rangle+7\langle T_Z\rangle}{3n_h}, \qquad (4)$$

where $\langle L_z\rangle$ is the expectation value of the angular momentum operator of the *d* states, $\langle S_z\rangle$ that of the spin operator, $\langle T_Z\rangle$ that of the magnetic dipole operator which accounts for the asphericity of the spin moment, $n_h$ the number of holes in the *d* band, and finally $\mu_0$ the absorption coefficient for the unpolarized x-ray radiation. The $\langle T_Z\rangle$ is negligible only for cubic structures,[29,48] but can account for up to 50% of the effective spin magnetic moment at the (001) surface of Ni.[27] So we expect it to be important for the $C1_b$ crystalline structure. To derive these sum rules several approximations are made with most important the ignorance of the interatomic hybridization, which is reflected on the nontreatment of the energy dependence of the radial matrix elements.

We apply the sum rules to the theoretical spectra for NiMnSb and PtMnSb, which are the most studied systems. The calculated spin magnetic moment is an effective one, as we do not separate the $\langle S_z\rangle$ term from the $\langle T_Z\rangle$ one. Results together with the direct calculations of the magnetic moments can be seen in Table III. The number of holes in the *d* band is calculated by integrating the element and *l* projected density of states inside each muffin-tin sphere. For the cutoff energy used as upper limit for the integrals in Eqs. (3) and (4), we integrate the density of states to find the number of holes. We found a value of 4 eV for Ni and 6 eV for the Mn and Pt atoms, but calculated magnetic moments do not change significantly with the cutoff energy (less than 2% if we increase the cutoff energy by 2 eV) as was the case in Fe and Fe nitrides.[30] Of course, even if sum rules where derived with no approximation direct calculated values and the ones derived by applying the sum rules to the theoretical spectra would be different as we do not take into account physical processes like the core-hole recombination[45] and the Coster-Kronig decay. But their inclusion in calculations requires the treatment of a time dependent two-electron Green's function, whose formalism is heavily involved in *ab initio* calculations.

As we can see in Table III direct and sum rules derived spin magnetic moments are in good agreement for all the atoms. Difference should come mostly from the $\langle T_Z\rangle$ term as $C1_b$ crystalline structure is highly anisotropic. It is remarkable that for Pt and Ni sites the sum rules have only slightly overestimated the spin magnetic moment and for Mn site slightly underestimated it as compared to direct calculations. The surprising agreement between the sum rules derived moments and the direct calculations is also reproduced in the case of the orbital magnetic moments with the exception of Mn in NiMnSb where orbital magnetic moment is positive in the direct calculations and negative when using the sum

rules, showing the sensitivity of the sum rules over the totality of the approximations used to derive them and the physical processes that were not included in the computation of the XMCD spectra. The agreement of the sum rule derived magnetic moments with the direct calculations using Eq. (1) is then not expected.

## VII. CONCLUSION

We have studied by means of a relativistic full-potential *ab initio* linear muffin-tin orbitals (LMTO) method the electronic structure and the x-ray magnetic circular dichroism for five Heusler alloys. The total energy calculations within the generalized-gradient approximation to the exchange-correlation potential produced equilibrium lattice constants that differ less than 1.2% from the experimental values. For NiMnSb and PtMnSb the main features of our density of states (DOS) agree well with previous studies, showing a gap in the minority spin band at the Fermi level and a large exchange splitting for the Mn $3d$ states. We showed that PdMnSb is not a half ferromagnet at ambient pressure but becomes one at higher hydrostatic pressure. PtMnSn has similar characteristics as PtMnSb but as it has one valence electron less, the Fermi level is lower in energy. Instead of a half metallic gap there exists a region of low spin-down DOS at the Fermi level and this gap is moved towards higher energies. The PtMnTe alloy shows very low total DOS just before the Fermi level and consequently a semimetallic behavior.

The x-ray-absorption spectra (XAS) of the Pt atoms in the different Pt-based alloys are similar, while the x-ray magnetic circular dichroism (XMCD) spectra change significantly reflecting the underlying changes in the electronic structure and induced magnetic moments. Mn atoms show the same behavior in all the compounds but as the number of the valence electrons increases the $2p$ core states become deeper by about 1 eV. The theory underestimates the $L_3/L_2$ integrated branching ratio compared to experiment at the Mn site in NiMnSb and PtMnSb, and reproduces only qualitatively the XAS spectrum of Ni in NiMnSb. Finally, for Pd no XMCD experiments are available yet so that our calculations of XAS and XMCD remain a prediction. The good agreement between the directly calculated magnetic moments and the ones derived by applying the sum rules to the theoretical spectra is surprising and not expected since the sum rules are derived for atoms.

## ACKNOWLEDGMENTS

I.G. was supported by the European Union Grant No. ERBFMXCT96-0089. One of us (S.O.) acknowledges financial support from a grant by ''Le Ministere de l'Education Nationale, de la Recherche et de la Technologie'' of France. The calculations were performed using the facilities of the SGI Origin-2000 supercomputer of the Université Louis Pasteur of Strasbourg and the IBM SP2 supercomputer of CNUSC under Grant No. gem1917.

[1] F. Heusler, Verh. Dtsch. Phys. Ges. **5**, 219 (1903).
[2] R. A. de Groot, F. M. Mueller, P. G. van Engen, and K. H. J. Buschow, Phys. Rev. Lett. **50**, 2024 (1983).
[3] K. Watanabe, Trans. Jpn. Inst. Met. **17**, 220 (1976).
[4] *Magnetic Properties of Non-Metallic Inorganic Compounds Based on Transition Elements*, edited by H. P. J. Wijn, Landolt-Börnstein, New Series, Group III, Vol. 27, Pt. a (Springer, Berlin, 1988), p. 385.
[5] P. G. van Engen, K. H. J. Buschow, R. Jongebreuer, and M. Erman, Appl. Phys. Lett. **42**, 202 (1983).
[6] J. A. Caballero, Y. D. Park, A. Cabbibo, R. Childress, F. Petroff, and R. Morel, J. Appl. Phys. **81**, 2740 (1997).
[7] M. C. Kautzky and R. M. Clemens, in *Magnetic Ultrathin Films, Multilayers and Surfaces*, edited by A. Fert, H. Fujimori, G. Guntherodt, B. Heinrich, W. E. Egelhoff, Jr., E. E. Marinero, and R. L. White, MRS Symposia Proceedings No. 384 (Materials Research Society, Pittsburgh, 1995), p. 109; M. C. Kautzky and R. M. Clemens, Appl. Phys. Lett. **66**, 1279 (1995); M. C. Kautzky, F. B. Mancoff, J.-F. Bobo, P. R. Johnson, and R. L. White, J. Appl. Phys. **81**, 4026 (1997).
[8] K. E. H. M. Hanssen and P. E. Mijnarends, Phys. Rev. B **34**, 5009 (1986).
[9] E. T. Kulatov and I. I. Mazin, J. Phys.: Condens. Matter **2**, 343 (1990).
[10] O. K. Andersen, Phys. Rev. B **12**, 3060 (1975).
[11] S. J. Youn and B. I. Min, Phys. Rev. B **51**, 10 436 (1995).
[12] X. Wang, V. P. Antropov, and B. N. Harmon, IEEE Trans. Magn. **30**, 4458 (1994).
[13] U. von Barth and L. Hedin, J. Phys. C **5**, 1629 (1972).
[14] M. M. Kirillova, A. A. Makhnev, E. I. Shreder, V. P. Dyakina, and N. B. Gorina, Phys. Status Solidi B **187**, 231 (1995).
[15] J. F. Bobo, R. J. Johnson, M. Kautzky, F. B. Mancoff, E. Tuncel, R. L. White, and B. M. Clemens, J. Appl. Phys. **81**, 4164 (1997).
[16] H. Ebert and G. Schütz, J. Appl. Phys. **69**, 4627 (1991).
[17] M. J. Otto, R. A. M. van Woerden, P. J. van der Valk, J. Wijngaard, C. F. van Bruggen, and C. Haas, J. Phys.: Condens. Matter **1**, 2351 (1989).
[18] X. Gao, J. A. Woolam, R. D. Kirby, D. J. Sellmyer, C. T. Tanaka, J. Nowak, and J. S. Moodera, Phys. Rev. B **59**, 9965 (1999).
[19] V. N. Antonov, P. M. Oppeneer, A. N. Yaresko, A. Ya. Perlov, and T. Kraft, Phys. Rev. B **56**, 13 012 (1997).
[20] J. van Ek and J. M. MacLaren, Phys. Rev. B **56**, R2924 (1997).
[21] *Core Level Spectroscopies for Magnetic Phenomena: Theory and Experiment*, edited by P. S. Bagus, G. Pacchioni, and F. Parmigiani (Plenum, New York, 1995).
[22] *Spin-Orbit Influenced Spectroscopies of Magnetic Solids*, edited by H. Ebert and G. Schütz, Lecture Notes in Physics Vol. 466 (Springer-Verlag, Heidelberg, 1996).
[23] B. T. Thole, P. Carra, F. Sette, and G. van der Laan, Phys. Rev. Lett. **68**, 1943 (1992).
[24] P. Carra, B. T. Thole, M. Altarelli, and X. Wang, Phys. Rev. Lett. **70**, 694 (1993).
[25] G. van der Laan, Phys. Rev. B **57**, 112 (1998).
[26] C. T. Chen, Y. U. Idzerda, H.-J. Lin, N. V. Smith, G. Meigs, E. Chaban, G. H. Ho, E. Pellegrin, and F. Sette, Phys. Rev. Lett. **75**, 152 (1995).

[27] R. Wu, D. Wang, and A. J. Freeman, Phys. Rev. Lett. **71**, 3581 (1993); R. Wu and A. J. Freeman, *ibid.* **73**, 1994 (1994).
[28] A. Kimura, S. Suga, T. Shishidou, S. Imada, T. Muro, S. Y. Park, T. Miyahara, T. Kaneko, and T. Kanomata, Phys. Rev. B **56**, 6021 (1997).
[29] H. Ebert, Rep. Prog. Phys. **59**, 1665 (1996).
[30] M. Alouani, J. M. Wills, and J. M. Wilkins, Phys. Rev. B **57**, 9502 (1998).
[31] C. Brouder and M. Hikam, Phys. Rev. B **43**, 3809 (1991); Ch. Brouder, M. Alouani, and K. H. Bennemann, *ibid.* **54**, 7334 (1996).
[32] G. Y. Guo, Phys. Rev. B **57**, 10 295 (1998).
[33] A. L. Ankudinov and J. J. Rehr, Phys. Rev. B **56**, 1712 (1997).
[34] G. van der Laan and B. T. Thole, Phys. Rev. B **43**, 13 401 (1991).
[35] J. M. Wills and B. R. Cooper, Phys. Rev. B **36**, 3809 (1987); M. Alouani and J. M. Wills, *ibid.* **54**, 2480 (1996).
[36] J. P. Perdew and Y. Wang, Phys. Rev. B **33**, 8800 (1986); **45**, 13 244 (1992).
[37] W. Grange, I. Galanakis, M. Alouani, M. Maret, J.-P. Kappler, and A. Rogalev (unpublished).
[38] I. Galanakis, S. Ostanin, M. Alouani, H. Dreyssé, and J. M. Wills, Phys. Rev. B **61**, 599 (2000).
[39] M. J. Otto, R. A. M. van Woerden, P. J. van der Valk, J. Wijngaard, C. F. van Bruggen, C. Haas, and K. H. J. Buschow, J. Phys.: Condens. Matter **1**, 2341 (1989).
[40] Otto *et al.* (Ref. 39) synthesized polycrystalline samples at 1500 °C by electric-arc melting of the component elements. To interpret their x-ray powder-diffraction results they supposed that their samples are completely ordered. Only PtMnSn showed a strongly atomic disorder (atoms not in the correct site), but their results did not allow them to obtain reliable quantitative results for this disorder.
[41] Notice that the projected DOS is calculated inside each muffin-tin sphere, since the interstitial region cannot be easily divided between atoms. In addition the polarization of the interstitial region is very weak and we found that it contributes $\pm 0.05\mu_B$ at the most to the total spin magnetic moment and hence it is not important for the discussion of the magnetic properties.
[42] S. V. Halilov and E. T. Kulatov, J. Phys.: Condens. Matter **3**, 6363 (1991).
[43] P. Hohenberg and W. Kohn, Phys. Rev. **136**, B864 (1964); W. Kohn and L. J. Sham, *ibid.* **140**, A1133 (1965).
[44] M. S. S. Brooks, Physica B **130**, 6 (1985); G. Vignale and M. Resalt, Phys. Rev. B **37**, 10 685 (1988).
[45] J. Schwitalla and H. Ebert, Phys. Rev. Lett. **80**, 4586 (1998).
[46] I. Galanakis, S. Ostanin, M. Alouani, H. Dreyssé, and H. Ebert (unpublished).
[47] A. Ankudinov and J. J. Rehr, Phys. Rev. B **51**, 1282 (1995).
[48] G. Y. Guo, H. Ebert, W. M. Temmerman, and P. J. Durham, Phys. Rev. B **50**, 3861 (1994).